J Neurophysiol 97: 4327–4340, 2007.
First published April 25, 2007; doi:10.1152/jn.01091.2006.

Functional Circuitry for Peripheral Suppression in Mammalian Y-Type Retinal Ganglion Cells

Kareem A. Zaghloul,[1] Michael B. Manookin,[3] Bart G. Borghuis,[1] Kwabena Boahen,[2] and Jonathan B. Demb[1,3,4,5]

[1]*Departments of Neuroscience and* [2]*Bioengineering, University of Pennsylvania, Philadelphia, Pennsylvania; and* [3]*Neuroscience Program and* [4]*Departments of Ophthalmology and Visual Sciences and* [5]*Molecular, Cellular and Developmental Biology, University of Michigan, Ann Arbor, Michigan*

Submitted 11 October 2006; accepted in final form 22 April 2007

Zaghloul KA, Manookin MB, Borghuis BG, Boahen K, Demb JB. Functional circuitry for peripheral suppression in mammalian Y-type retinal ganglion cells. *J Neurophysiol* 97: 4327–4340, 2007. First published April 25, 2007; doi:10.1152/jn.01091.2006. A retinal ganglion cell receptive field is made up of an excitatory center and an inhibitory surround. The surround has two components: one driven by horizontal cells at the first synaptic layer and one driven by amacrine cells at the second synaptic layer. Here we characterized how amacrine cells inhibit the center response of ON- and OFF-center Y-type ganglion cells in the in vitro guinea pig retina. A high spatial frequency grating (4–5 cyc/mm), beyond the spatial resolution of horizontal cells, drifted in the ganglion cell receptive field periphery to stimulate amacrine cells. The peripheral grating suppressed the ganglion cell spiking response to a central spot. Suppression of spiking was strongest and observed most consistently in OFF cells. In intracellular recordings, the grating suppressed the subthreshold membrane potential in two ways: a reduced slope (gain) of the stimulus-response curve by ~20–30% and, in OFF cells, a tonic ~1-mV hyperpolarization. In voltage clamp, the grating increased an inhibitory conductance in all cells and simultaneously decreased an excitatory conductance in OFF cells. To determine whether center response inhibition was presynaptic or postsynaptic (shunting), we measured center response gain under voltage-clamp and current-clamp conditions. Under both conditions, the peripheral grating reduced center response gain similarly. This result suggests that reduced gain in the ganglion cell subthreshold center response reflects inhibition of presynaptic bipolar terminals. Thus amacrine cells suppressed ganglion cell center response gain primarily by inhibiting bipolar cell glutamate release.

INTRODUCTION

The retina represents a model system for understanding how neural circuitry generates the receptive field properties of sensory neurons. Ganglion cells are the output neuron of the retina and have been well characterized at the level of extracellular recording. A receptive field typically features a center region, which can be excited by an effective stimulus (Enroth-Cugell and Robson 1966; Kuffler 1953). For an ON-center cell, the effective stimulus is a brightening over the center, whereas for an OFF-center cell, the effective stimulus is a dimming over the center. Under cone-driven conditions, the receptive field center primarily corresponds to a feed-forward pathway from cones to bipolar cells to the ganglion cell (Fig. 1) (Masland 2001; Sterling and Demb 2004; Wässle 2004). The ganglion cell center shows an approximately Gaussian spatial profile, which arises from the dome-like distribution of bipolar synapses onto the ganglion cell dendritic tree (Kier et al. 1995).

The receptive field center response is suppressed by stimulation of the surround (Kuffler 1953) (Fig. 1). In the classical description, the surround represents a broad region extending across and beyond the center (Enroth-Cugell and Robson 1966; Rodieck 1965). This classical surround exhibits poor spatial resolution and therefore senses low spatial frequencies, including broad-field stimuli and low spatial-frequency gratings. In addition to the classical surround, the ganglion cell center can be suppressed by high spatial frequency contrast patterns in the peripheral receptive field. This peripheral suppression can be distinguished from the classical surround based on spatial resolution. For example, the spiking response to a central spot can be suppressed by peripheral contrast, such as high spatial frequency drifting gratings (~1 cycle/° or ~4–5 cycles/mm on the retina), that would not stimulate the classical surround (Caldwell and Daw 1978a,b; Enroth-Cugell and Jakiela 1980; Lankheet et al. 1992; Shapley and Victor 1979; Solomon et al. 2006). Peripheral suppression is not equally strong in all cell types but is particularly prominent in the brisk-transient cell types, which include the parasol/magnocellular pathway cells in primates and α/Y-type cells in other mammals (Caldwell and Daw 1978a,b; Enroth-Cugell and Jakiela 1980; Shapley and Victor 1979; Solomon et al. 2006).

Surround mechanisms are created at both synaptic layers in the retina (Fig. 1). At the outer plexiform layer, horizontal cells inhibit cones and bipolar cells (Fig. 1) (Duebel et al. 2006; Lankheet et al. 1992; Mangel 1991; McMahon et al. 2004). Horizontal cells are electrically coupled to one another in a syncytium (Baldridge et al. 1998). Thus the horizontal cell network has requisite properties to convey the classical surround mechanism, sensitive to low spatial frequency stimuli. At the inner plexiform layer, amacrine cells inhibit bipolar cell synaptic terminals and ganglion cell dendrites (Fig. 1). Amacrine cells are driven by bipolar cells, which themselves have relatively narrow receptive fields that would yield sensitivity to high spatial frequencies (Dacey et al. 2000). Furthermore, a nonlinearity at the bipolar cell synapse creates a subunit structure in postsynaptic cells and extends sensitivity to high spatial frequencies (Demb et al. 2001a; Hochstein and Shapley 1976). Thus an amacrine cell mechanism for surround inhibition

Address for reprint requests and other correspondence: J. Demb, Univ. of Michigan, Kellogg Eye Center, 1000 Wall St., Ann Arbor, MI 48105 (E-mail: jdemb@umich.edu).

The costs of publication of this article were defrayed in part by the payment of page charges. The article must therefore be hereby marked "*advertisement*" in accordance with 18 U.S.C. Section 1734 solely to indicate this fact.

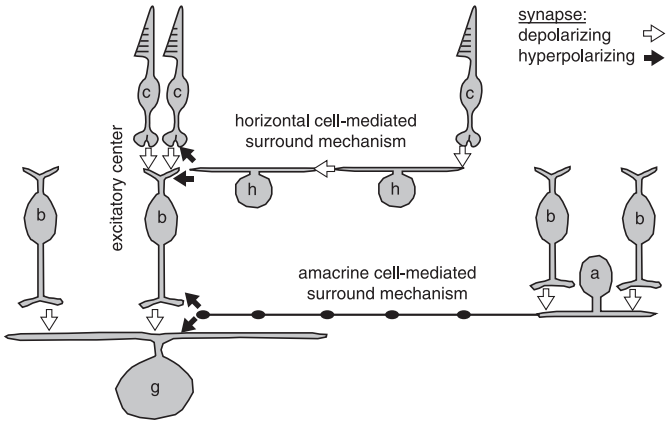

FIG. 1. Circuitry for receptive field center and surround mechanisms. Excitatory receptive field (RF) center response of the ganglion cell (g) arises from cone photoreceptors (c) releasing glutamate onto bipolar cells (b), which in turn release glutamate onto the ganglion cell (g). A split into ON and OFF pathways arises at the cone synapse, where postsynaptic bipolar cells express either ionotropic glutamate receptors (OFF pathway), which preserve the sign of cone response, or metabotropic receptors (ON pathway), which invert the sign of cone response (Sterling and Demb 2004). Surround arises partly from cone-driven horizontal cell (h) feedback. Horizontal cells excite neighboring cells through gap junctions and ultimately inhibit cones and bipolar cells that make up the center pathway. Surround also arises from bipolar cell-driven amacrine cell (a) feedback. Amacrine cell-mediated inhibition can act directly onto the ganglion cell and onto the presynaptic bipolar terminal. Shown is the circuit for an OFF-center ganglion cell; the ON-center cell would have a similar circuit except that cone synapses are hyperpolarizing.

would be sensitive to both low and high spatial frequencies (Cook and McReynolds 1998; Cook et al. 1998; Demb et al. 1999; Flores-Herr et al. 2001; Taylor 1999).

Here, we asked how amacrine cell inhibition acts to suppress the center response of a ganglion cell. To this end, we presented high spatial frequencies in the ganglion cell's receptive field periphery to selectively stimulate amacrine pathways. Direct measurements showed that such frequencies only minimally stimulate horizontal cells. Therefore the suppressive effects measured in the ganglion cell must be driven by amacrine circuitry. An amacrine cell's inhibitory signal can reach the ganglion cell either directly, through a synapse on the dendrite, or indirectly, through a synapse onto a presynaptic bipolar terminal (Cook and McReynolds 1998; Cook et al. 1998; Flores-Herr et al. 2001; Shields and Lukasiewicz 2003; Taylor 1999). Here, we tested the relative contributions of these two synaptic sites and determined their individual roles in the suppression of the excitatory center response of the ganglion cell.

METHODS

Tissue preparation

For each experimental session, a retinal whole mount (flattened eye cup) was prepared from a Hartley guinea pig (200–800 g). Procedures were in accordance with University of Pennsylvania, University of Michigan, and National Institutes of Health guidelines. In some cases, an animal was anesthetized with ketamine (100 mg/kg), xylazine (20 mg/kg), and pentobarbital (150 mg/kg), and both eyes were removed, after which the animal was killed by anesthetic overdose. In other cases, an animal was anesthetized with ketamine (40 mg/kg) and xylazine (4 mg/kg) and decapitated, and both eyes were removed. Each eye was hemisected, and the vitreous was peeled off in one piece. Five slits were cut, so that the eye cup would lay flat. The flattened eye cup, which included the neural retina attached to the pigment epithelium, choroid, and sclera, was mounted on a piece of circular filter paper and mounted flat in a chamber on a microscope stage. The filter paper was held in place by a teflon ring that fit tightly in the chamber walls. The tissue was superfused (~4–6 ml/min) with oxygenated (95% O_2-5% CO_2) Ames medium (Sigma, St. Louis, MO) at 32–36°C (Demb et al. 1999). In some experiments, glucose was added to the medium (0.8–3.6 g/l); this increased osmolarity by ~2–6% and did not have noticeable effects on the recordings.

Electrophysiology

For intracellular recordings of ganglion cells, Acridine orange (0.001%; Molecular Probes, Eugene, OR) was added to the superfusate, allowing ganglion cell somas to be identified by fluorescence during brief exposure to UV light. A soma in the visual streak was penetrated with a glass electrode (tip resistance, 80–200 MΩ) filled with 1% pyranine (Molecular Probes) in 2 M potassium acetate. Voltage was recorded with an intracellular amplifier (NeuroData, IR-283, NeuroData Instruments, Delaware Water Gap, PA) and digitized at 5 kHz using AxoScope software (Axon Instruments, Foster City, CA). For horizontal cells, recordings were obtained with glass electrodes (impedance, 80–200 MΩ) back-filled with Alexa 488 or 568 and neurobiotin (5%) in 1.5 M potassium acetate. Membrane potential was amplified (NeuroData, IR-283), sampled at 2 kHz, and digitized by a computer for on-line analysis and storage (Apple Macintosh; 10-bit AD board; custom built software). Resting potential was recorded after cell penetration and continuously monitored during the recording. After the recording, horizontal cells were injected with the dye and fixed for confocal microscopy.

For extracellular (loose-patch) and whole cell recordings from ganglion cells, we identified large somas visualized with a cooled CCD camera (Retiga 1300C, QCapture software, Qimaging, Burnaby, British Columbia, Canada) (Hu et al. 2000). Positive pressure was applied through a patch electrode (3–6 MΩ) and filled with Ames medium, and this electrode was used to "burrow" through the inner limiting membrane and clean the area surrounding the targeted cell (Roska and Werblin 2001). The same electrode was used to form a loose seal onto the targeted cell (~30–100 MΩ) and record spikes under voltage clamp (V_{hold} = 0 mV). This electrode was withdrawn, and a second electrode (3–6 MΩ) filled with intracellular solution was used to obtain a >1-GΩ seal. The patch was ruptured, and recordings were made in the whole cell configuration. Intracellular solution for current-clamp recordings contained (in mM) 140 K methylsulfate, 8 NaCl, 10 HEPES, 0.1 EGTA, 2 ATP-Mg, and 0.3 GTP-Na_2, adjusted to pH 7.3. For voltage-clamp recordings, QX-314-Br was added (5 mM) to block sodium channels and improve space clamp, and NaCl was reduced to 3 mM. The calculated reversal for inhibitory responses ($E_{GABA/glycine}$) would be approximately −73 mV for the first solution. For the second solution, containing Br^-, $E_{GABA/glycine}$ should be more depolarized given that GABA/glycine channels are more permeable to Br^- than Cl^- by ~20% (Bormann et al. 1987; Robertson 1989). In calculations below, we assumed that with Br^- in the pipette, $E_{GABA/glycine}$ was approximately −68 mV. Junction potential (−9 mV) was corrected in all cases.

For voltage-clamp recordings, the holding potential was compensated for the voltage drop across the electrode tip, based on the following equation: $V_{h\_corr} = V_h - [I_{leak} R_s (1 - R_{s\_correct})]$, where V_h is the apparent holding potential before the stimulus (in mV), I_{leak} is the leak current (in nA), R_s is the series resistance (typically 12–30 MΩ), and $R_{s\_correct}$ is the series resistance compensation (typically between 0.25 and 0.50). Holding potentials were typically restricted to a range negative to −30 mV; positive to −30, the cells showed a large outward current, which resembled a delayed-rectifier potassium current. Signals were recorded with a MultiClamp 700A amplifier and digitized at 10 kHz using pClamp 9.0 software (Axon Instruments).

Programs were written in Matlab (Mathworks, Natick, MA) to analyze responses (downsampled to 1 kHz) separately in the spike rate and subthreshold membrane potential, as described previously (Demb et al. 2001a; Zaghloul et al. 2003, 2005). To exclude the spikes from the voltage response, we down-sampled the raw data (recorded at 5 or 10 kHz) by taking the median value of every 5 or 10 sample points; this had the effect of removing spikes but preserving the subthreshold waveform. In some cells, we instead used a linear interpolation method, where we clipped out each spike with a line from 1 ms before to 1–2 ms after each spike (Zaghloul et al. 2003).

Data are reported as mean ± SE. Statistical significance was assessed using a one-tailed *t*-test.

Horizontal cell morphology

After recording horizontal cells, the retina was fixed in 4% paraformaldehyde for 20 min. Cells were visualized either based on the Alexa dye staining or by reacting for Neurobiotin by the following procedure: incubate with blocking buffer (10% normal goat serum, 5% Triton-X in 5% sodium phosphate buffer, 1 h); react with streptavidin-fluorescein (8 mg/ml) or streptavidin-Cy5 (40 mg/ml) for 3 h; wash with 5% sodium phosphate buffer (3 × 10 min); mount on a slide using Vectashield (Vector Laboratories, Burlingame, CA). Cells were imaged using a confocal microscope (Leica, Nussloch, Germany; ×40 objective; NA, 1.25).

Visual stimulus

The stimulus was displayed on a miniature monochrome computer monitor (Lucivid MR1-103, Microbrightfield, Colchester, VT) projected through a microscope port and through a ×2.5 or ×4 objective focused on the photoreceptors. The monitor had a vertical refresh of 60 Hz and a spatial resolution of 640 × 480. The stimulus was confined to the central 480 × 480 pixels, which, when projected onto the retina, subtended 3 × 3 or 3.7 × 3.7 mm. The mean luminance was $\sim 10^3$-10^4 isomerizations per middle-wavelength sensitive cone or rod per second, which is within the mesopic rang (Yin et al. 2006); in two cases, a lower mean luminance was used ($\sim 10^2$ isomerizations per cone or rod per second). The relationship between gun voltage and monitor intensity was linearized in software with a lookup table. Stimuli were programmed in Matlab as described previously (Brainard 1997; Demb et al. 1999; Pelli 1997).

All ganglion cell experiments used a dynamic modulation of a low-contrast spot (diameter, 0.5 mm) centered on the cell body and therefore approximately centered on both the dendritic tree and the ~0.5- to 0.7-mm-diam receptive field center (Demb et al. 2001a,b; Dhingra et al. 2003). The spot will necessarily stimulate both the classical center and the surround, because these overlap in space (Enroth-Cugell and Robson 1966). However, the purpose of the spot was to stimulate the bipolar cells that synapse onto the ganglion cell dendritic tree, and for this purpose, the spot, even if centering was off by ~0.1 mm, would be adequate to stimulate most of these bipolar cells.

The spot intensity was updated at 60 Hz, with values drawn randomly from a Gaussian distribution. This stimulus approximates "white noise" (Marmarelis and Marmarelis 1978; Sakai and Naka 1987; Fig. 2). The stimulus distribution is presented in contrast units, where the intensity has been normalized by subtracting the mean luminance and dividing by the mean luminance. Thus the stimulus had a mean of 0 and a range of −1 to +1. Stimulus contrast is defined by the Gaussian SD, which was always 0.10. The stimulus lasted 240 s and included twelve 20-s periods: 10 s of the spot (spot alone) alternating with 10 s of the spot plus a drifting grating (spot + grating). The grating was presented in the periphery, excluded from a 1-mm patch centered on the cell body. The grating had a square-wave profile with a spatial frequency of 4.3 or 5.0 cycles/mm (bar width = 116 or 100 μm), a temporal frequency of 2 Hz, and a contrast of 1.0. The analysis was performed on data collected during the last 8 s of each 10-s half-period. Thus for each contrast, there was 8 × 12 = 96 s of data. This relatively short stimulus increased the probability of highly stable intracellular recordings and provided data with sufficient signal-to-noise for the analysis. Because of the alternating contrast half-periods, any instabilities during the recording should be distributed equally between the two half-periods. Horizontal cell recordings used drifting sine-wave gratings (2 Hz, 0.7 contrast, 0.05–6 cycles/mm) presented over a field of 2.4 × 3.2 mm.

Analysis: linear-nonlinear model

We analyzed both subthreshold and spiking responses using a linear-nonlinear (LN) cascade analysis (Carandini et al. 2005; Chichilnisky 2001). In this analysis, a linear filter represents the impulse response function of a cell, or the theoretical response to a brief light flash (Fig. 2). This filter, plotted in reverse, represents the cells weighting function. The linear prediction of the response (i.e., the linear model) is calculated at a given point in time by multiplying the stimulus by the weighting function and summing the result (i.e., convolution; Carandini et al. 2005). To compute the L filter, $f(t)$, we cross-correlated the stimulus and the response (Chichilnisky 2001; Lee and Schetzen 1965; Sakai et al. 1995; Wiener 1958). To generate the L model of response (r_L), we convolved (*) the stimulus [$s(t)$] and the L filter

$$r_L(t) = f(t)*s(t)$$

Finally, the L model is passed through a nonlinear input–output function to generate a LN model of the response (Fig. 2)

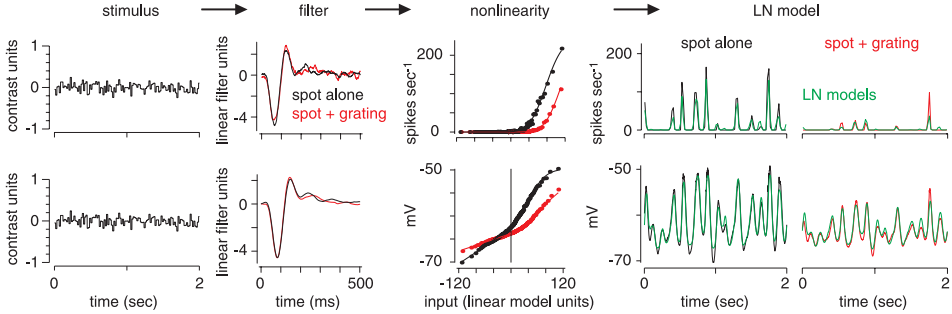

FIG. 2. Linear-nonlinear (LN) model of spiking and subthreshold membrane potential responses. Stimulus (in contrast units) is convolved with a linear filter to generate linear model of response. Linear model (in input units) is passed through an instantaneous (static) nonlinearity to generate the LN model of the response (in spikes/s or mV). Model (green lines), built from 1 data set, can be compared with average response to a brief test stimulus (black or red lines) from a separate data set (averaged over 24 repeats to reduce noise). Model corresponds closely to data. Shown are models for spiking (*top row*) and subthreshold membrane potential responses (*bottom row*) to spot alone and spot + grating conditions. The r^2 between model and data was 0.88 (spikes, spot alone); 0.67 (spikes, spot + grating); 0.95 (membrane potential, spot alone); and 0.91 (membrane potential, spot + grating).

$$r_{LN}(t) = N[r_L(t)]$$

The N function accounts for rectification (e.g., the spike threshold) and saturation in the response (Baccus and Meister 2002; Chichilnisky 2001; Kim and Rieke 2001; Sakai et al. 1995; Victor 1987; Zaghloul et al. 2003).

To generate the N function, we plotted the L model versus the actual response (analyzed after down-sampling to 1 kHz) and binned the data (~1000 samples/bin). These binned points represent the average response output (in spikes/s, mV, or pA) at each level of the L model value (in arbitrary input units). For the simultaneous fitting procedure described below, we required a descriptive function fitted through the points of the N function. A Gaussian cumulative distribution function (cdf) provides a good fit to the spike N function (Chander and Chichilnisky 2001; Zaghloul et al. 2003, 2005)

$$f(x) = \alpha C(\beta x + \gamma)$$

where (C) is the cumulative normal density, x is the input value, and the parameters roughly correspond to the maximum response (α), the response gain (β), and the spike threshold (γ) (Chander and Chichilnisky 2001; Chichilnisky 2001). The fit was performed using standard routines in Matlab that minimize the mean-squared error (MSE) between the data and the fitted line (Fig. 2). For the membrane N points, we fit the data with the function

$$f(x) = \alpha C(\beta x + \gamma) + \delta$$

where the additional parameter δ allows for a vertical offset (because the membrane N function goes negative). As we found previously, the Gaussian cdf provided a good fit for the membrane potential N function for ON cells but not for OFF cells (Zaghloul et al. 2003). Thus for OFF cells, we fit the positive and negative sides of the membrane N function separately (Zaghloul et al. 2003, 2005).

Analysis: simultaneous fit of spike responses to the spot alone and spot + grating conditions

There is a free scale factor in the LN model: the y-axis of the filter and the x-axis of the nonlinear function can be scaled by the same amount without changing the output of the model (Chander and Chichilnisky 2001; Kim and Rieke 2001; Zaghloul et al. 2005). Therefore to compare between the two conditions, we initially multiplied each filter by a factor, so that the variance of the two linear models was equal (Baccus and Meister 2002). We scaled the nonlinearities by the same factors (i.e., a stretch along the x-axis) so that each LN model output remained unchanged. After normalizing in this way, the two filters showed only slight differences in kinetics, but there was a large difference between the N functions: the peripheral grating typically reduced the spike rate, which resulted in an apparent rightward shift of the N function.

We considered three models to explain the effect of the peripheral grating on the N stage of the model. First, we considered a gain change model in which the two curves were fit with the same Gaussian cdf, except for a scaling along the x-axis. Specifically, both curves were fit with the same α and γ parameters, but unique β parameters (i.e., total of four parameters). This model was used previously to account for the reduced gain evoked by an increase in the contrast of the spot itself (Beaudoin et al. 2007; Chander and Chichilnisky 2001; Kim and Rieke 2001; Zaghloul et al. 2005). However, based on a preliminary analysis of OFF cells, it was apparent that this model failed in a systematic way: an underestimation of the small amplitude responses to the spot alone and an overestimation of the small amplitude responses in the presence of the grating. Therefore we considered a threshold change model in which the two curves were fit with the same Gaussian cdf except for a horizontal shift along the x-axis. Specifically, both curves were fit with the same α and β parameters, but unique γ parameters (i.e., total of four parameters). Finally, we considered a combined model that allowed for both a gain change and a threshold change. Specifically, both curves were fit with the same α parameters but unique β and γ parameters (i.e., total of 5 parameters).

The gain change and threshold change models have the same form and equal number of parameters so we could directly compare the MSE of these models to determine which provided a better fit to the data. The combined model has an additional parameter and so we expect it to yield a lower MSE. However, the combined model allowed us to test whether the gain change or threshold change dominated in explaining the difference between the two contrast curves when both gain and threshold were allowed to vary.

Analysis: simultaneous fit of subthreshold responses to the spot alone and spot + grating conditions

For membrane potential or current responses, we fit both low and high contrast N functions with the Gaussian cdf plus offset. The low and high contrast functions were fit with the same α and γ parameters but unique β and δ parameters. Thus the fitted N functions were similar to those for the spike N functions, except that membrane potential N functions were allowed to have unique offsets (i.e., unique y-intercepts because of the unique δ). The unique offsets were necessary, because in some cases, the y-intercept of the membrane N function differed between contrasts by several millivolts or tens of picoamperes (Baccus and Meister 2002). Furthermore, the gain change between conditions (change in β) was independent of the change in the y-intercept. For ON cells, we performed the simultaneous fit with the cdf to the full nonlinear function, whereas for OFF cells, we fit just the excitatory (depolarizing or inward current) side of the nonlinear function (Zaghloul et al. 2003, 2005). For the subthreshold response, the above gain change model showed good fits, without systematic errors of any sort, and so we did not consider alternative models as we did for the spike response.

Evaluation of the LN model

The LN model is useful to the extent that it provides an accurate representation of a cell's response. We evaluated model accuracy by building the model based on data collected with one stimulus and testing the model's predictive power (explained variance: r^2) on the averaged response to a second stimulus. The model-building stimulus was a modulated spot, as described above: twelve 20-s periods (10 s of spot alone and 10 s of spot + grating). The model-testing stimulus was a 2-s segment of spot modulation, repeated 10 times in a 20-s period (10 s of spot alone and 10 s of spot + grating). The model-testing period (MT) was interspersed six times within the model building periods (MB): 3 MT; 2 MB; 3 MT; 2 MB; 3 MT; 2 MB; and 3 MT. In all cases, we only analyzed the last 8 s of data from each 10-s half-period. Thus the LN model was built from 96 s of data for both spot alone and spot + grating conditions. The response to the 2-s model-testing segment was averaged over 24 repeats for both spot alone and spot + grating conditions. We tested how well the LN model predicted the averaged response to the 2-s model-testing segment (Fig. 2). The model was assessed in this way for 14 cells (11 OFF cells and 3 ON cells) and for both spiking and subthreshold measurements. For spiking responses, we evaluated the model in cases where the firing rate was at least 1 spike/s for both conditions. We evaluated model fits for the theshold change model, which generally yielded better fits than the gain change model.

For spiking responses, the r^2 between the LN model and the data were 0.80 ± 0.03 for the spot alone condition and 0.65 ± 0.03 for the spot + grating condition (n = 13). For membrane potential responses, the r^2 between the LN model and the data were 0.94 ± 0.01 for the spot alone condition and 0.90 ± 0.01 for the spot + grating condition (n = 11). Thus the LN model generally gave a better fit for the spot alone condition than for the spot + grating condition, although this

difference was most marked for spiking responses; membrane potential responses were very well captured by the LN model in either condition. The relatively low r^2 value for spiking response to the spot + grating condition was likely caused by the lower spike rates in this condition.

RESULTS

Basic cellular properties

We targeted Y-type (α) ganglion cells, because these cells show significant peripheral suppression in vivo and because we could identify them routinely by their large cell bodies in the visual streak (Caldwell and Daw 1978b; Demb et al. 1999, 2001a; Enroth-Cugell and Jakiela 1980; Peichl et al. 1987). We presented a series of stimuli to confirm that the cell had the characteristic properties: a "brisk-transient" center response to a spot (0.5 mm diam), an antagonistic surround response to an annulus (inner diameter, 0.74; outer diameter, 2.0 mm), and a nonlinear (frequency-doubled) response to a contrast-reversing grating (spatial frequency = 4.3 or 5.0 cycles/mm) (Cleland and Levick 1974; Demb et al. 2001a,b; Enroth-Cugell and Robson 1966; Hochstein and Shapley 1976). In whole cell recordings, cells had an input resistance of 32 ± 3 (SE) MΩ (n = 17), similar to our previous measurements and similar to Y-types cells in the cat retina (Beaudoin et al. 2007; Cohen 2001; Manookin and Demb 2006; O'Brien et al. 2002; Zaghloul et al. 2003).

Here we report on 65 ganglion cells (48 OFF-center and 17 ON-center). As in previous studies, we had a bias toward successful recordings from OFF-center cells (Zaghloul et al. 2003, 2005), which outnumber their ON-center counterparts by about twofold (B. Borghuis, unpublished observations). We recorded extracellularly from 36 cells (26 OFF-center and 10 ON-center), which, when viewing a gray screen at mean luminance, fired spontaneously at 10 ± 3 spikes/s (range = 0–57). We recorded intracellularly from 32 cells (25 OFF-center and 7 ON-center), which fired spontaneously at 5 ± 2 spikes/s (range = 0–49) and rested at −64.1 ± 0.9 mV. Ten cells were recorded with sharp intracellular electrodes, and 22 were recorded with whole cell patch electrodes. We made additional whole cell recordings with QX-314 (5 mM) added to the pipette solution to block spiking (n = 13 cells). Some cells were recorded by both extracellular and intracellular methods (n = 23 cells). Our main criteria for stable intracellular recordings were a low resting potential and a well-modulated light response to the flickering spot stimulus described below.

Spatial tuning of horizontal cells in the guinea pig retina

We recorded horizontal cells to assess their spatial sensitivity in the guinea pig retina. Here we report on cells that were successfully filled with a fluorescent dye to identify the type (A-type or B-type; Peichl and Gonzalez-Soriano 1993). At mean luminance, horizontal cells rested at −47 ± 5 mV (n = 30). Responses were recorded to sine-wave gratings at a range of spatial frequencies; the response was quantified as the amplitude of the best fitting sine-wave at the 2-Hz drift frequency (F1 amplitude). Maximal response amplitudes were 3.8 ± 0.5 (A-type; n = 24) and 3.2 ± 1.1 mV (B-type; n = 6). Both types of horizontal cell showed low-pass spatial sensitivity with half-maximal sensitivities near 0.4–0.5 cycles/mm

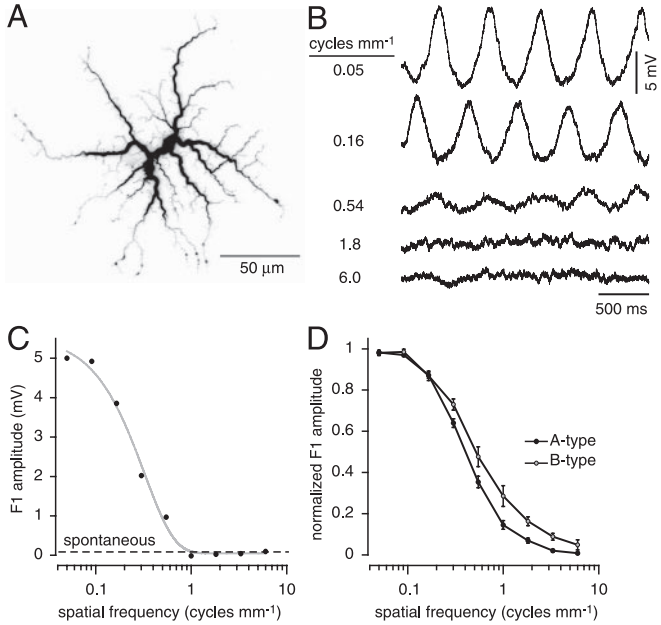

FIG. 3. Spatial bandwidth of horizontal cells. *A*: A-type horizontal cell in the visual streak of guinea pig retina. Fluorescence image was converted to grayscale, and contrast was inverted. *B*: intracellular responses of the cell in *A* to drifting sine-wave gratings at various spatial frequencies (0.7 contrast). Each trace shows average of 2 repetitions. Resting potential was −47 mV. *C*: Cell's spatial transfer function is low-pass with a half-maximal response at ~0.2 cyc/mm (same cell as in *A* and *B*). Responses are F1 amplitudes at each spatial frequency. Smooth gray line shows a sigmoidal fit (Matlab; least-squares method). Dashed line shows F1 amplitude to a blank screen (spontaneous). *D*: average spatial transfer functions for a population of A-type and B-type horizontal cells. Responses have been normalized by subtracting spontaneous response and dividing by maximal response. At 5 cyc/mm, responses are attenuated to <10% of the peak response.

(Fig. 3*D*). At 5 cycles/mm, the response declined to ~4 (HA cells, n = 24) or ~7% (HB cells, n = 6) of the peak response (Fig. 3*D*). In the following experiments, we used spatial frequencies of 4.3 or 5.0 cycles/mm. At these frequencies, the bar width (~100 μm) should match the putative width of a bipolar cell receptive field, which drive amacrine cells but is too fine to strongly stimulate horizontal cells (Fig. 3) (Dacey et al. 2000; Demb 1999, 2001a,b; Lankheet 1992; Passaglia et al. 2001; Werblin 1972).

Peripheral contrast suppresses the ganglion cell spiking response to a central stimulus

We first quantified the effect of the peripheral grating on the ganglion cell receptive field center as measured in the spike response. To stimulate the cell, a 0.5-mm-diam spot flickered over the center; on each frame of the monitor (16.7 ms), an intensity value was drawn randomly from a Gaussian distribution (see METHODS and Fig. 4*A*). This stimulus approximates white noise, with approximately equal stimulus energy over the range of temporal frequencies to which the cell is most sensitive (Zaghloul et al. 2005). In alternate 10-s half-cycles, the spot was presented either alone or in the presence of a grating in the peripheral receptive field (Fig. 4*A*). During the 10-s presentation, the grating drifted at 2 Hz and thus maintained a constant contrast signal at each point in the periphery (Enroth-Cugell and Jakiela 1980).

The central spot, presented alone, caused a series of spike bursts in the ganglion cell, and this spiking was suppressed by

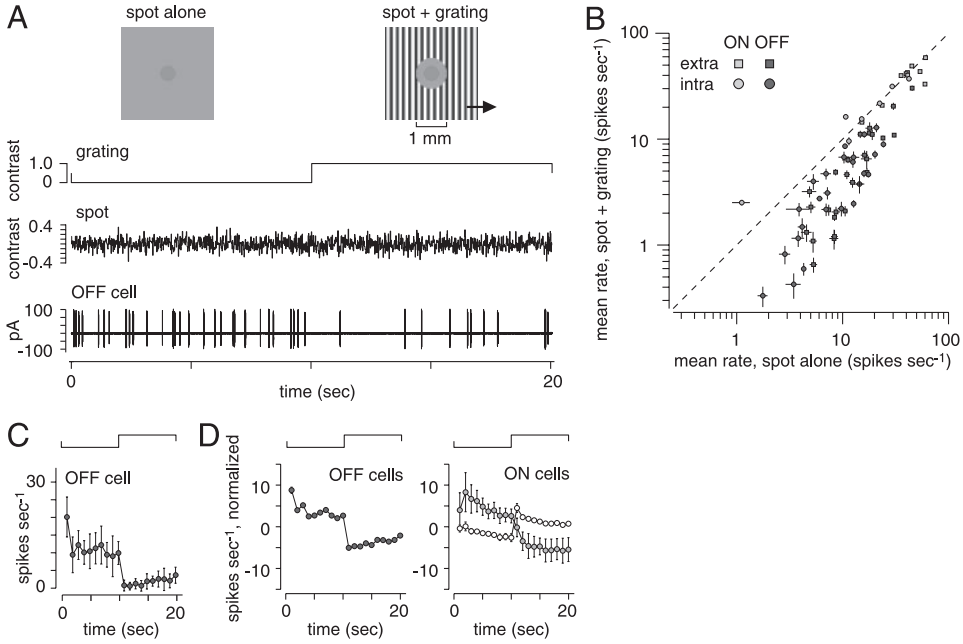

FIG. 4. Peripheral contrast suppresses spiking responses to a central spot. *A*: ganglion cell extracellular response to 1 cycle of stimulus protocol (bottom trace). Each cycle consisted of a 10-s period of a flickering spot (0.5 mm diam, centered on ganglion cell body) followed by a 10-s period of spot plus a drifting grating in the periphery; spot and grating time-courses are indicated above trace. Grating was excluded from a central patch (1 mm diam; see image at *top*). Grating was full contrast with 100-μm-wide bars and a 2-Hz drift rate. Grating suppressed spiking response to the spot. *B*: effect of grating on firing rate in individual cells. Plotted are firing rates during the last 8 s of each half-cycle. Grating reduced firing rate in all OFF cells and in some ON cells (points below dashed identity line). Error bars indicate ±SE across 12 cycles. *C*: firing rate across 20-s stimulus cycle, averaged across 12 cycles (same cell as *A*). Error bars indicate ±SD across cycles. Line above data, here and in *D*, indicates grating time-course (as in *A*). *D*: normalized spiking response across the 20-s stimulus cycle. Normalized response is firing rate at each point in stimulus cycle minus average rate over entire cycle. *Left*: average for 44 OFF cells, all of which showed a significant decrease in firing rate during grating. *Right*: average of 5 ON cells that showed a decreased spike rate (gray symbols) and 7 ON cells that showed an increased spike rate during grating (white symbols). Error bars indicate ±SE across cells.

the addition of the peripheral grating. Similar results were observed in spiking responses recorded by extracellular and intracellular methods, and so results on spiking, here and below, were combined across recording conditions. We analyzed the effect of the grating on the spike rate over the last 8 s of each 10-s half-cycle. For OFF cells, the spike rate reduced from 12.2 ± 1.3 to 5.6 ± 0.8 spikes/s, a drop of 6.7 ± 0.6 (n = 44 cells, 26 extracellular; $P < 0.001$). For ON cells, the spike rate reduced from 32 ± 4 to 30 ± 4 spikes/s, a drop of 1.8 ± 1.9 (n = 16 cells and 10 extracellular; not significant; Fig. 4*D*). We further quantified the effect of the grating by testing for a significant reduction in spiking within individual cells. For each cell, we compared the spike rate between the two conditions across the 12 cycles and performed a t-test (2-tailed). For every OFF cell, the grating significantly reduced the firing rate ($P < 0.01$ for 41 cells; $P < 0.05$ for 3 cells; Fig. 4, *B* and *D*). For ON cells, the grating significantly reduced the rate in five cells ($P < 0.05$), had no significant effect in four ($P > 0.05$), and significantly increased the rate in seven ($P < 0.05$; Fig. 4, *B* and *D*); the increased rate in some ON cells could result from inadvertent stimulation of the edge of the receptive field center. Thus the grating consistently reduced the spike rate in OFF cells but had a more variable effect in ON cells.

Peripheral contrast causes the linear filter to become more biphasic in OFF-center cells

To further quantify the impact of the peripheral grating on the center response, we analyzed the spike train with an LN analysis (see METHODS and Fig. 2). The goal of the LN analysis was to separate changes in the temporal sensitivity of the cell from changes in contrast sensitivity (Carandini et al. 2005; Chichilnisky 2001). The linear filter indicates the temporal sensitivity of the cell. The nonlinear function shows the relationship between the filtered contrast (i.e., the linear model of the response) and the output of the cell; the slope of this function indicates the contrast sensitivity (see METHODS). For the spike response, we restricted our analysis to those cells that fired at a rate of at least 1 spike/s in both conditions and cells that showed a significant reduction in firing rate during the spot + grating condition (n = 40 OFF cells and 5 ON cells).

For OFF cells, the grating caused the linear filter to become more biphasic (Fig. 5*C*). To quantify the change in the shape of the filter, we compared the amplitude of the first phase of the response (i.e., positive response for ON cells; negative response for OFF cells), with the second phase of the response (i.e., negative response for ON cells; positive response for OFF cells). We calculated a biphasic index, which was the second phase amplitude (s_2 or sg_2 for the spot alone or spot + grating) divided by the first phase amplitude (s_1 or sg_1). If there were no second phase of the response, the index would be zero, whereas if the second phase amplitude equaled the first phase amplitude, the index would be −1. Most cells, with or without the peripheral grating present, had an index between −0.2 and −1.0 (Fig. 5*C*).

For OFF cells (n = 40 cells), the biphasic index was −0.55 ± 0.02 for the spot alone condition compared with −0.73 ± 0.03 for the spot + grating condition, a difference of −0.17 ± 0.02 ($P < 0.001$). For ON cells (n = 5 cells), the biphasic index was

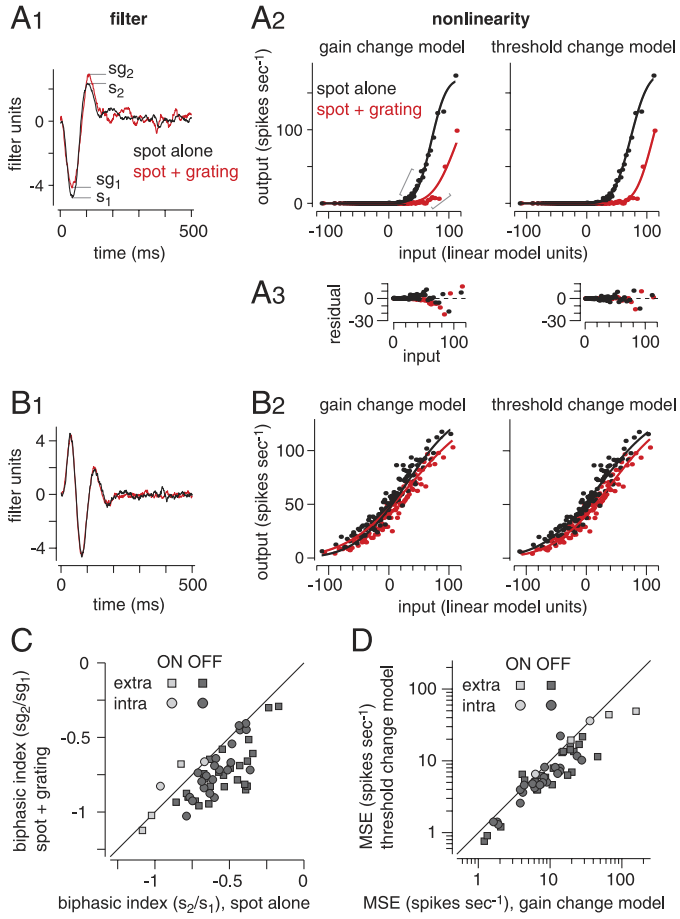

FIG. 5. Peripheral contrast changes response kinetics and increases threshold for spiking consistently in OFF cells. *A1*: linear filter for spot alone and spot + grating conditions. Peripheral grating caused the filter to become more biphasic. To quantify biphasic nature of the filter, we measured amplitude of the 1st phase of the filter (negative response for OFF cells, positive for ON cells) for both the spot alone (s_1) and spot + grating condition (sg_1) and compared this with amplitude of the 2nd phase of the filter (positive response for OFF cells, negative for ON cells) for spot alone (s_2) and spot + grating condition (sg_2). Filters are from the OFF cell in Fig. 4*A*. *A2*: nonlinearity for spot alone and spot + grating conditions. Data points show binned spike rate as a function of linear model values. Data are fit (smooth lines) with Gaussian cumulative distribution functions (cdfs) that are identical except for a scale factor that stretches curves along the *x*-axis (gain change model) or shifts curves laterally along *x*-axis (threshold change model). The threshold change model fit the data with a lower mean squared error (MSE; 4.7 spikes/s) than the gain change model (10.7 spikes/s). The gain change model underestimated small responses in the spot alone condition and overestimated small responses in spot + grating condition (gray brackets). *A3*: residuals (difference between data and fit) from *A2*. *B1*: same format as *A1* for an ON cell. Grating did not evoke a change in the shape of the filter. *B2*: same format as A2 for an ON cell. Data were better described by the threshold change model than the gain change model in this cell. *C*: population analysis of effect of peripheral grating on response kinetics. Grating caused OFF cells to become more biphasic (points below identity line). ON cells were relatively unaffected. Pattern of results (here and in *D*) was consistent for spikes measured with extracellular (extra) and intracellular (intra) recordings. Analysis here and in *D* was restricted to those cells that fired at a rate of at least 1 spike/s for both conditions and for which grating caused a significant suppression of spike rate ($n = 40$ OFF cells, $n = 5$ ON cells). *D*: the threshold change model best explains suppression of spiking in presence of peripheral grating for OFF cells. Plot shows MSE for the gain change and threshold change models. Most OFF cell points fall below the identity line, indicating that the threshold change model yields lower MSE. ON cells were about equally well fit by the 2 models.

-0.91 ± 0.07 for the spot alone condition compared with -0.86 ± 0.09 for the spot + grating condition, a difference of -0.05 ± 0.04 (not significant). Thus the peripheral grating caused the linear filter to become more biphasic in OFF cells but had no significant effect in ON cells. The increased biphasic quality of the OFF cell filter, caused by the peripheral grating, should correspond to a relatively decreased sensitivity to low temporal frequencies.

Peripheral suppression in OFF cells is best explained by an increased spike threshold

We next compared the effect of the grating on the spiking nonlinear function. We considered two models, with an equal number of parameters (4), to describe the suppression of spiking caused by the grating. In the first model, the grating causes a gain change. The reduced gain corresponds to a reduced slope of the nonlinear function. We also considered a second model, in which the grating causes an increased threshold for spiking (threshold change model). This increased threshold corresponds to a rightward shift (on a linear axis) in the nonlinear function in the spot + grating condition (see METHODS). For an OFF cell, the threshold change model provided a more satisfactory fit (Fig. 5*A*). We also considered a combined model, with an additional parameter (5), in which the two nonlinear functions differed by both their gain (slope) and their threshold (horizontal position along the *x*-axis).

To quantify the difference between the gain change model and the threshold change model, we fit both models for each cell and compared the difference in MSE between each model and the data. For OFF cells ($n = 40$ cells), the threshold change model yielded lower MSE (7.2 ± 0.8 spikes/s) compared with the gain change model (11.1 ± 1.4 spikes/s); the MSE was relatively lower for the threshold change model by $27 \pm 4\%$ ($P < 0.001$). The combined model fit yielded a lower MSE (6.8 ± 0.7 spikes/s) compared with the models above, as expected based on the additional parameter added in the fit. However, the MSE for the combined model was only slightly lower than that for the threshold change model above. Furthermore, in the combined model fit, the relative gain in the presence of the grating was 0.98 ± 0.02 (i.e., reduction of ~2%), and thus a gain change did not play a major role in describing the suppressed spiking. In the combined model, the threshold change (i.e., rightward shift) was 23.8 ± 1.4 arbitrary (linear model) units, similar to that found using the threshold change model (23.3 ± 1.5 units). Thus for OFF cells, the effect of the grating could be described concisely as an increased spike threshold.

For ON cells ($n = 5$), the MSE was not significantly lower for the threshold change model (31 ± 8 spikes/s) compared with the gain change model (57 ± 27 spikes/s); the threshold change model was lower by $19 \pm 14\%$ (not significant). For the combined model (MSE = 28 ± 7 spikes/s), the peripheral grating caused both a significant gain reduction (0.85 ± 0.03; i.e., reduction of ~15%) and an increased threshold (rightward shift, 19 ± 6 units). Thus for this subset of ON cells (which showed significantly reduced firing during the grating), the effect of the grating could be described as a combination of an increased spike threshold and a reduced gain.

In the preceding experiments, the grating was always presented at full contrast (1.0). In six OFF cells, we further tested

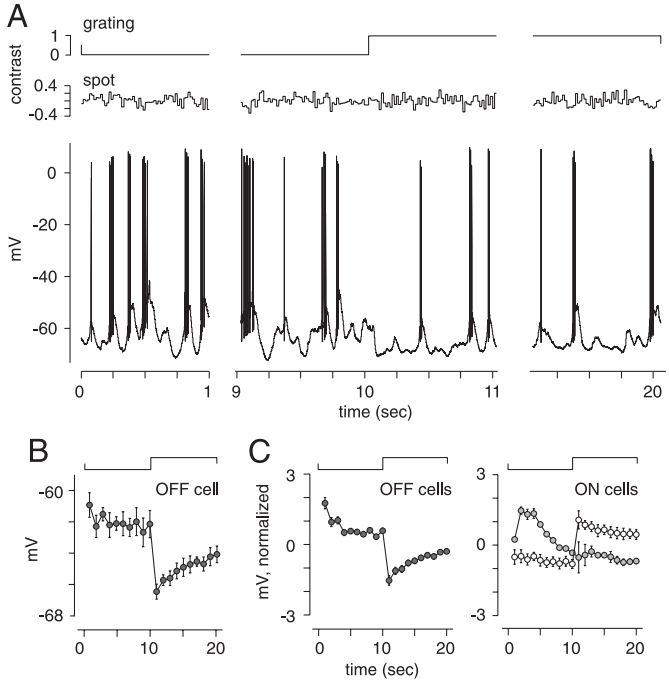

FIG. 6. Peripheral contrast hyperpolarizes the membrane potential in OFF cells. *A*: OFF ganglion cell intracellular response to 1 cycle of the stimulus protocol; shown are the 1st second, the middle 2 s, and the last second of the 20-s cycle. *B*: average subthreshold membrane potential across the 20-s stimulus cycle (same cell as *A*). Grating caused a hyperpolarization that partially recovered during the 10-s half-cycle. Error bars indicate ±SD across cycles. *C*: normalized membrane potential across the 20-s stimulus cycle. Normalized response is membrane potential at each point in stimulus cycle minus average membrane potential over entire cycle. *Left*: average for 25 OFF cells. *Right*: average of 2 ON cells that showed a hyperpolarization (gray symbols) and 3 ON cells that showed a depolarization during the grating (white symbols). Error bars indicate ±SE across cells.

the effect of the grating at a lower contrast (0.25). Data were analyzed using the threshold change model. For these cells, the low contrast grating caused a rightward shift of the nonlinear function of 8 ± 2 linear model units at low contrast and 20 ± 3 units at high contrast. Thus there was a significant effect of the grating at low contrast with a significantly greater effect at high contrast (difference of 12 ± 2 units; $P < 0.01$). Therefore at the lower contrast level, the effect of the grating was not saturated.

Peripheral contrast causes tonic membrane hyperpolarization in OFF cells

To understand the mechanism underlying the above effects on spiking, we analyzed the effect of the peripheral grating on the subthreshold membrane potential. In OFF cells, the grating evoked a tonic membrane hyperpolarization (Fig. 6). The hyperpolarization was largest at the onset of the peripheral stimulus and slowly declined over the 10-s half-cycle. During the period of analysis (2–10 s after grating onset or offset), the grating hyperpolarized the membrane potential from −64.6 ± 0.9 to −65.7 ± 0.8 mV, a difference of 1.2 ± 0.2 mV ($n = 25$ cells; $P < 0.001$). At the offset of the peripheral stimulus, the membrane initially depolarized strongly, and this depolarization declined during the half-cycle (Fig. 6*C*).

Individual ON cells showed either a tonic depolarization or hyperpolarization, so that the average effect of the grating on membrane potential was negligible. The membrane potential was −59.7 ± 2.6 mV during the spot alone and −59.4 ± 2.5 mV in the presence of the grating ($n = 7$). ON cells that showed a depolarization during the grating corresponded to those that showed an increased spike rate (see above and Fig. 4*B*), whereas cells that showed a hyperpolarization corresponded to those that showed a decreased spike rate ($n = 5$; Fig. 6*C*). As discussed below, the depolarization in some ON cells probably arises from unintended stimulation of excitatory bipolar cell synapses at the edge of the ganglion cell's receptive field center (see DISCUSSION).

Peripheral contrast reduces the response gain of subthreshold responses

In addition to tonic hyperpolarization of the membrane potential, the peripheral grating suppressed the amplitude of response fluctuations to the central spot (Fig. 6*A*). To quantify the nature of this suppression, we performed an LN analysis of the subthreshold response, similar to the analysis described above for the spike rate. Two LN models were fit that allowed, between conditions, a tonic membrane polarization (difference

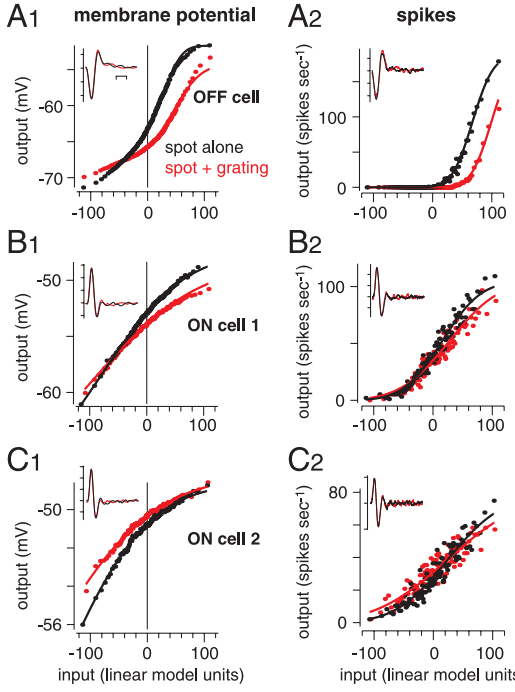

FIG. 7. Peripheral contrast reduces gain of subthreshold responses. *A1*: linear filter and static nonlinearity for membrane potential response to spot alone and spot + grating conditions. *Inset*: linear filters for the 2 conditions (normalized to have equal variance; scale bar indicates 100 ms; *y*-axis is in arbitrary filter units). Points show the 2 static nonlinearities. Depolarizing (rightward) sides of nonlinearities were fit with Gaussian cdfs that differed by a gain change (i.e., scaling along the *x*-axis) and a tonic hyperpolarization (i.e., vertical shift, reflected by a drop in *y*-intercept). Grating reduced gain by 36% and hyperpolarized membrane by 2.6 mV. Data are a whole cell recording of the OFF cell in Fig. 6*A*. *A2*: analysis of spiking response for cell in *A1*. Threshold change model was fit to data (rightward shift of 32 input units). *B1*: same as *A1* for an ON cell. Grating reduced gain by 23% and hyperpolarized membrane by 1.0 mV. *B2*: analysis of spiking response for the cell *B1*. Combined model was fit to data (reduced gain by 21%; rightward shift of 12 input units). *C1*: same as B1 for a 2nd ON cell. Grating reduced gain by 21% and depolarized membrane by 0.4 mV. *C2*: analysis of spiking response for cell in *C1*. Combined model was fit to data (reduced gain by 27%, leftward shift of 1 input unit).

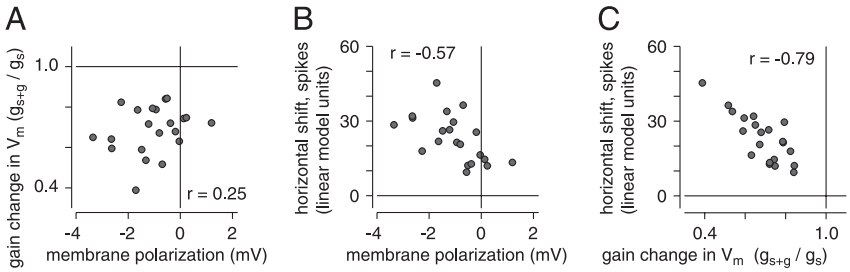

FIG. 8. Peripheral contrast effects on subthreshold and spiking responses are correlated. *A*: relationship between effect of grating on average membrane potential and reduced gain of membrane potential ($n = 21$ OFF cells with firing rates of at least 1 spike/s in both conditions). Change in average membrane potential was measured as change in the *y*-intercept of nonlinear function (negative values indicate that peripheral grating caused hyperpolarization). Gain change shows gain in the spot + grating condition (g_{s+g}) relative to gain in the spot alone condition (g_s). Correlation was not significant. *B*: relationship between effect on average membrane potential and horizontal shift in spike nonlinearity (positive values indicate rightward shift in presence of grating). Correlation was significant ($P < 0.05$). *C*: relationship between reduced gain in membrane potential and horizontal shift in spike nonlinearity. Correlation was significant ($P < 0.01$).

in the *y*-intercept of the nonlinearity) plus a gain change (difference in the slope of the nonlinearity; see METHODS). The example OFF cell shows the typical effect: the grating caused both hyperpolarization and a reduced gain (Fig. 7*A*; see also Fig. 2). The accompanying spike response is shown with the threshold change model fitted to the data (Fig. 7*A*; see also Fig. 2). For ON cells, there were two patterns. In the first pattern, the grating caused a hyperpolarization and reduced gain, similar to the OFF cell (Fig. 7*B*). In the second pattern, the grating caused a depolarization and reduced gain (Fig. 7*C*). The accompanying spike responses for the two ON cells are shown with the combined model fitted to the data (Fig. 7, *B* and *C*). For both patterns, the grating reduced the slope of the spike nonlinearity, but the rightward shift of the spike nonlinearity was only present in the case where the grating evoked hyperpolarization (Fig. 7*B*).

Next, we compared quantitatively the reduced gain during the spot + grating conditions across cells. For every cell recorded intracellularly ($n = 25$ OFF cells and 7 ON cells), the grating reduced the gain of the subthreshold response. For OFF cells, the gain was reduced significantly below 1.0 to 0.68 ± 0.02 ($P < 0.001$; i.e., reduction of ~32%). For ON cells, the gain was reduced to 0.78 ± 0.06 ($P < 0.001$; i.e., reduction of ~22%). The change in the *y*-intercept is a measure of membrane polarization, independent of the nonlinearity. The *y*-intercept showed a hyperpolarization for OFF cells (−1.0 ± 0.2 mV; $P < 0.001$), similar to the direct analysis of membrane potential above, but no significant change for ON cells (+0.3 ± 0.4 mV). Thus the reduced gain in the membrane potential response, observed in all cells, was not always accompanied by membrane hyperpolarization. The apparent independence of these two inhibitory effects suggests distinct underlying cellular mechanisms.

To further analyze the relationship between the suppressive effects on spiking and subthreshold responses, we measured three correlations. This analysis was performed on OFF cells, where the effect of the grating on spiking could be described concisely as an increased threshold; the analysis was further restricted to those OFF cells that fired at a rate of at least 1 spike/s for both conditions ($n = 21$ cells). There was not a significant correlation between the reduced gain in the subthreshold response and the hyperpolarization (i.e., the change in the *y*-intercept of the nonlinear function; Fig. 8*A*). Thus these two effects on the subthreshold response could arise from different cellular mechanisms; we further support this conclusion with analyses below. The rightward shift of the spike response was correlated with both the hyperpolarization ($r = -0.57$; $P < 0.05$) and the reduced gain in the subthreshold response ($r = -0.79$; $P < 0.01$; Fig. 8, *B* and *C*). Thus the suppression of the spiking response was related to both suppressive effects expressed in the subthreshold potential.

Peripheral contrast increases ganglion cell membrane conductance

We tested whether the hyperpolarization in OFF cells, caused by the peripheral grating, could be explained by a direct inhibitory synapse onto the ganglion cell dendrite. To test this, we made intracellular recordings with QX-314 in the pipette to block spiking and improve the space clamp. We measured the response to the peripheral grating in voltage clamp at several holding potentials. Every cell showed an increased conductance (i.e., positive slope on the *I-V* plot) during both the transient and sustained periods of the grating (Fig. 9). For OFF cells ($n = 6$), the conductance increased by 8 ± 2 nS for the transient response and 1.3 ± 0.4 nS for the sustained response. The transient response reversed at −94 ± 4 mV, and the sustained response (2–10 s after grating onset) reversed at −97 ± 18 mV.

The above reversal potential measurements suggest that, for OFF cells, the grating simultaneously increased an inhibitory conductance ($\Delta g_{GABA/glycine}$) and decreased an excitatory conductance (Δg_{cation}), which would move the reversal potential for the summed conductance (Δg_{total}) negative to $E_{GABA/glycine}$. To determine the relative contributions of the two underlying conductances [where the conductances represent changes (Δ) from resting conductances], we used the following formula

$$a = (E_{GABA/glycine} - E_{total})/(E_{total} - E_{cation})$$

where a is the ratio between the conductances ($\Delta g_{cation}/\Delta g_{GABA/glycine}$), $E_{GABA/glycine} = -68$ mV, $E_{cation} = 0$ mV, and E_{total} was the measured reversal potential for the leak-subtracted response to the grating. The above equation follows from Ohm's law, given that, during the sustained period of the grating, $\Delta i_{cation} = -\Delta i_{GABA/glycine}$. From this equation, we could divide the total conductance into the two underlying conductances (after establishing their relative contributions). This procedure is depicted graphically in Fig. 9*C*. For OFF cells ($n = 6$), the grating evoked an inhibitory conductance of 1.7 ± 0.4 nS ($P < 0.05$; 2-tailed *t*-test) in parallel with a decreased excitatory conductance of 0.43 ± 0.14 nS ($P < 0.05$; Fig. 9*D*).

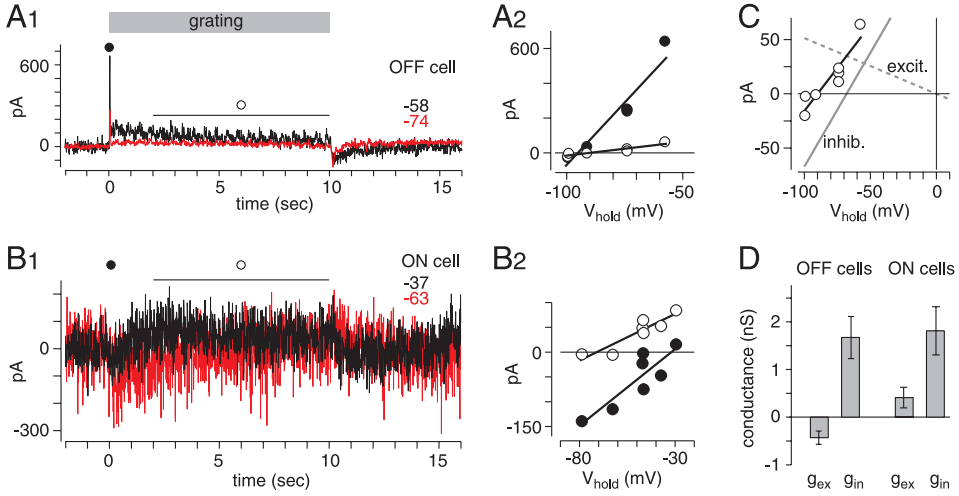

FIG. 9. Peripheral contrast causes an increased membrane conductance. *A1*: OFF cell response to peripheral grating was measured in voltage clamp: V_{hold} = −58 or −74 mV. Traces are leak-subtracted and show response to a single presentation of grating. *A2*: *I-V* plots show amplitude of transient current, right after grating onset (dark symbol), and sustained current during main period of analysis, 2–10 s after grating onset (white symbols). Lines show regression fits; *x*-intercept of fit is apparent reversal potential. This reversal was −95 (transient response) or −90 mV (sustained response). *B1*: same format as *A1* for an ON cell: V_{hold} = −37 or −63 mV. *B2*: same format as *A2* for ON cell in *B1*. Reversal was −32 (transient response) or −71 mV (sustained response). *C*: sustained response from *A2* is shown with calculated underlying excitatory (dashed gray line) and inhibitory conductances (solid gray line). The 2 underlying conductances, when summed, equal total conductance (i.e., regression fit to data; solid black line). *D*: average excitatory conductance (g_{ex}) and inhibitory conductance (g_{in}) during sustained response to grating for OFF cells (n = 6) and ON cells (n = 4). Error bars indicate ±SE.

For ON cells (n = 4), the conductance increased by 5 ± 3 nS for the transient response and 2.2 ± 0.6 nS for the sustained response. The transient response reversed at −29 ± 1 mV, and the sustained response reversed at −55 ± 6 mV. For the sustained response, the grating evoked an inhibitory conductance of 1.8 ± 0.5 nS ($P < 0.05$) in parallel with an increased excitatory conductance of 0.41 ± 0.22 nS (not significant; Fig. 9*D*). Therefore in all cells, the grating evoked an increased inhibitory conductance, consistent with a direct inhibitory synapse on the ganglion cell dendrite. This inhibitory conductance was accompanied either by a decreased excitatory conductance (OFF cells) or a trend toward an increased excitatory conductance (ON cells) that depended on cell type.

Evidence that peripheral contrast reduces the gain of subthreshold ganglion cell center responses by inhibiting presynaptic bipolar cells

We next tested whether the reduced gain of the subthreshold response could be explained by postsynaptic shunting inhibition or rather by presynaptic inhibition of bipolar terminals. To test this, we made intracellular recordings with QX-314 in the pipette, to block spiking and improve space clamp, and compared recordings of membrane current (I_m; with the holding potential, V_{hold}, near the resting potential) to recordings of membrane voltage (V_m). Consider first the voltage-clamp condition, where conductances in parallel would add. We considered the total membrane conductance as a sum of three conductances: synaptic conductance driven by the central spot (g_{center}), synaptic conductance driven by the peripheral grating ($g_{grating}$), and a leak term (g_{leak}), each with an associated reversal potential

$$I_m = g_{center}(V_{hold} - E_{center}) + g_{grating}(V_{hold} - E_{grating}) + g_{leak}(V_{hold} - E_{leak})$$

If the peripheral grating acts purely by postsynaptic inhibition, its effect would be exclusively on $g_{grating}$. During the analysis period (2–10 s after grating onset or offset), we expect $g_{grating}$ and g_{leak} to be relatively steady (Fig. 9), and we assume all reversal potentials to be constant. Thus an effect on $g_{grating}$ would evoke a tonic offset in current between the two conditions, with no additional effect on the gain of the center response, because the modulation amplitude of g_{center} would remain the same. If instead the peripheral grating acts through inhibition of the presynaptic bipolar terminal, in the equation above, the modulation amplitude of g_{center} itself would change, which should evoke a reduced gain under voltage clamp similar to that observed under current clamp. More generally, postsynaptic shunting inhibition, caused by tonic inhibitory synapses, should only be present under current clamp.

We used the LN model above to compare the effects of the grating on I_m and V_m (Fig. 10). Across 13 cells (n = 9 OFF cells and 4 ON cells), the reduction in gain was the same in both conditions: the grating reduced the center gain to 0.73 ± 0.04 (i.e., ~27% reduction) for I_m and to 0.72 ± 0.04 (i.e., 28% reduction) for V_m (Fig. 10). The effect was similar for OFF cells (V_m, 0.73 ± 0.03; I_m 0.74 ± 0.03) and ON cells (V_m, 0.70 ± 0.10; I_m 0.69 ± 0.10). These gain reductions in V_m are consistent with those recorded with standard pipette solution above (~22–32%). The reduced gain was accompanied in OFF cells by a slight hyperpolarization as reflected by a change in the *y*-intercept of the nonlinearity of −0.6 ± 0.5 mV (n = 9). This hyperpolarization was somewhat small and inconsistent across cells, compared with recordings above, perhaps caused by the more depolarized value for $E_{GABA/glycine}$ (i.e., with Br^- in the pipette solution) and the accompanying decreased driving force on inhibition (see METHODS). Under voltage clamp, OFF cells showed a small outward current (16 ± 13 pA). For ON cells, there was little change in the *y*-intercept under either condition (current clamp: −0.2 ± 0.7 mV; voltage clamp: 7 ± 28 pA). In general, our main conclusion from the comparison of current-clamp and voltage-clamp recordings is based on the similar reduction in gain across the two conditions. The reduced gain of the ganglion cell

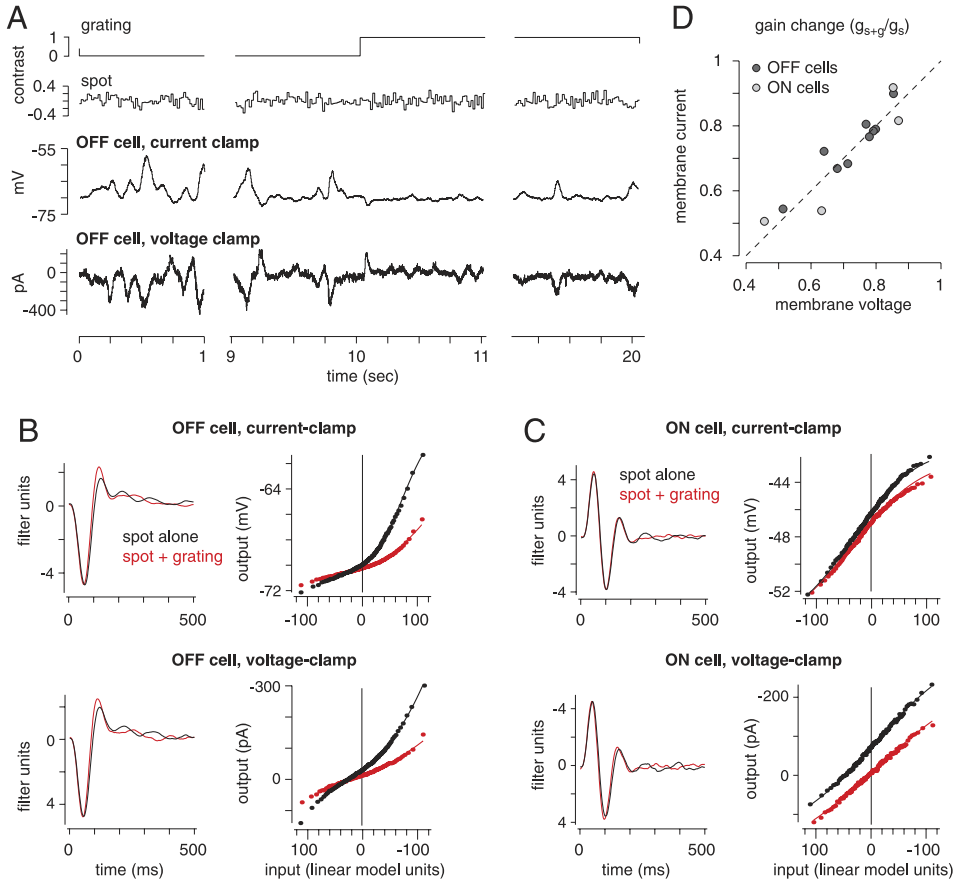

FIG. 10. Peripheral contrast reduces gain of subthreshold response similarly in membrane voltages and currents. *A*: time-course of effect of peripheral grating for an OFF cell measured in current clamp or voltage clamp (V_{hold} = −73 mV); same format as Fig. 6*A*. Recording solution included QX-314 to block sodium channels. *B*: linear-nonlinear model for OFF cell in *A*, measured in current clamp or voltage clamp. Grating reduced gain to a similar degree under current clamp (49%) and voltage clamp (46%). Fits to nonlinear functions are based on depolarizing responses (current clamp) or inward currents (voltage clamp). Note that for voltage-clamp recording here and in *C*, the *y*-axis of linear filter and both axes of nonlinearity have been plotted in reverse (i.e., negative values are going upward or rightward) to facilitate comparison with LN model for current-clamp recording. *C*: same as *B* for an ON cell. Grating reduced gain to a similar degree under current clamp (13%) and voltage clamp (18%; V_{hold} = −47 mV). *D*: across cells (n = 9 OFF cells, n = 4 ON cells), reduced gains measured under voltage-clamp and current-clamp conditions were similar. Gain change was measured in the spot + grating condition (g_{s+g}) relative to gain in the spot alone condition (g_s). Points lie near identity line.

center V_m response must be primarily caused by amacrine cell inhibition of presynaptic bipolar cell terminals.

DISCUSSION

We measured the effect of peripheral suppression on the center response of mammalian retinal ganglion cells using intracellular recording. We used a peripheral grating with a spatial frequency that was beyond the resolution of the horizontal cell network to selectively stimulate amacrine cells (Fig. 3). Our main finding was that the peripheral grating caused two suppressive effects on the ganglion cell subthreshold membrane potential: a reduced gain of the center response, evident in all cells (Figs. 7 and 8), and a tonic membrane hyperpolarization, most consistently observed in OFF cells (Figs. 6–8). The tonic membrane polarization was consistent with an increased inhibitory conductance at the ganglion cell dendrite in parallel with a decreased (OFF cells) or increased (ON cells) excitatory conductance (Fig. 9). For both cell types, the reduced gain of the center response was similar under current-clamp and voltage-clamp conditions, which suggests that this reduced gain reflects an inhibition of presynaptic bipolar terminals (Fig. 10).

Circuitry of amacrine-mediated peripheral suppression

A model explaining the main results is shown in Fig. 11. The drifting grating in the periphery stimulates bipolar cells, which each have a nonlinearity at their synaptic output (Demb et al. 2001a; Enroth-Cugell and Freeman 1987). Each bipolar cell then acts as a nonlinear subunit, which can increase its release more than it can decrease its release (i.e., rectification). The drifting bars stimulate the subunits asynchronously, which leads to a steady increase in the summed excitatory drive onto the amacrine cell (Demb et al. 2001a; Enroth-Cugell and Robson 1966; Hochstein and Shapley 1976; Olveczky et al. 2003). Tonic stimulation of the amacrine cell drives tonic inhibition of the recorded ganglion cell and its presynaptic bipolar cells. The long-range inhibitory signal is carried by a spiking amacrine cell, which fires conventional sodium spikes,

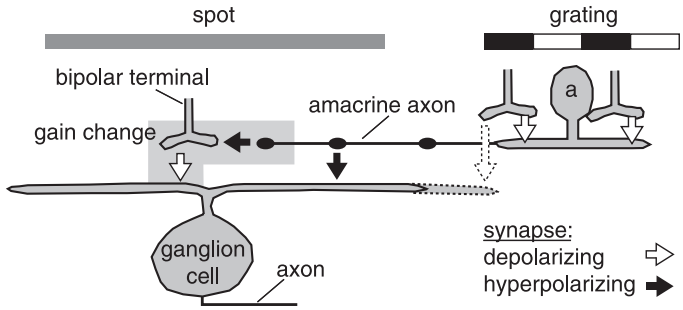

FIG. 11. Circuit model to explain influence of long-range amacrine signaling on ganglion cell center response. For OFF cells, amacrine cell inhibition acts at 2 points: a synapse onto the ganglion cell dendrite and a synapse onto the presynaptic bipolar cell terminal. Both synapses result in tonic hyperpolarization of the ganglion cell. Synapse on the bipolar terminal further causes a reduced gain of center response to the spot. For ON cells, the circuit would be similar except that, under these conditions, grating sometimes caused a tonic depolarization that could be explained by inadvertent stimulation of bipolar cells at the edge of the ganglion cell dendritic tree (arrow pointing from bipolar terminal to extended ganglion cell dendrite, in dashed lines).

blocked by TTX (Demb et al. 1999, 2001a; Flores-Herr et al. 2001; Olveczky et al. 2003; Roska and Werblin 2003; Taylor 1999). These amacrine cells are presumably those that extend axons millimeters across the retina (Dacey 1989; Famiglietti 1992; Stafford and Dacey 1997; Vaney et al. 1988). These long-range amacrine cells represent a class of cell that includes several types (Lin and Masland 2006; Volgyi et al. 2001). The specific types that synapse onto Y-type cells and their presynaptic bipolar terminals are unknown.

The reduced gain of the center response in the subthreshold membrane potential is apparently driven by amacrine cell inhibition of the central bipolar terminals (i.e., those conveying the spot response; Fig. 11). The hyperpolarization, shown most consistently in OFF cells, is driven by a combination of direct inhibition of the ganglion cell and inhibition of tonic glutamate release from presynaptic bipolar terminals (Figs. 9 and 11). For ON cells, the grating sometimes caused a slight depolarization that could be explained if the edge of the grating sometimes inadvertently caused direct stimulation of bipolar cells at the edge of the receptive field center (Figs. 6, 7, and 11). This may have occurred more frequently in ON cells because they are relatively larger than OFF cells in guinea pig retina, as found in primate and human parasol cells (Chichilnisky and Kalmar 2002; Dacey and Petersen 1992; J. Demb, unpublished observations). This inadvertent center stimulation may have also occurred in a few OFF cells and explain why the grating did not cause a tonic membrane hyperpolarization in all cases (Fig. 8*B*). Despite this variability in tonic membrane polarization, the grating reduced the gain of the center response in the subthreshold membrane potential for every ON and OFF cell studied. This suggests that the peripheral grating always evoked an inhibitory effect on those central-most bipolar terminals that conveyed the spot response.

Our data support two sites of synaptic inhibition driven by long-range amacrine cells: bipolar terminals and ganglion cells. This conclusion is consistent with previous studies in mammalian retina (Flores-Herr et al. 2001; Roska and Werblin 2003; Taylor 1999). However, we added to these previous efforts in four regards. First, we used a high spatial frequency surround stimulus and showed that it does not stimulate horizontal cells (Fig. 3). Thus surround effects studied here can be ascribed specifically to amacrine cells. Second, we used the LN model to study effects of amacrine cell stimulation on the temporal tuning of the center response. Under our conditions, effects on the temporal tuning were minimal. The grating caused a slightly more biphasic filter in OFF cells, which should attenuate low temporal frequencies (Fig. 5). Third, we used the LN model to quantify gain changes separately from static nonlinear (i.e., rectifying) influences on membrane voltage or current. Fourth, by directly comparing voltage-clamp and current-clamp recordings in the same cell, we determined whether shunting of the ganglion cell leads to reduced gain of the center response. The shunting effect was shown to be negligible (Fig. 10).

Comparing the circuit for peripheral suppression between mammals and lower vertebrates

The circuit revealed here in a mammalian retina shows both similarities and differences to a circuit proposed in lower vertebrate retina (Thibos and Werblin 1978; Werblin 1972; Werblin and Copenhagen 1974). In mudpuppy, a spinning windmill stimulus, like the drifting grating stimulus in this study, was shown to stimulate amacrine cells but not horizontal cells. The windmill stimulus, presented in the receptive field periphery, suppressed the spiking response of ganglion cells by causing a membrane hyperpolarization. However, in several studies, the windmill apparently did not suppress bipolar cells (Thibos and Werblin 1978; Werblin 1972; Werblin and Copenhagen 1974). Thus in mudpuppy, the amacrine cells seem to act mostly at the ganglion cell dendrite, whereas we showed here in a mammal an important role for suppression of the presynaptic bipolar terminals.

The amacrine cells that mediate the windmill-evoked suppression rely on sodium action potentials to convey signals laterally over long distances (Cook and Werblin 1994; Cook et al. 1998). Bath-applied TTX blocked suppression in ganglion cells but not bipolar cells in one study (Cook and McReynolds 1998; Cook et al. 1998). However, another study showed that inhibition at salamander bipolar terminals is TTX-sensitive (Shields and Lukasiewicz 2003). Thus there may be a role for presynaptic inhibition in the salamander circuit for peripheral suppression similar to the presynaptic mechanism shown here. In ON-OFF ganglion cells, the OFF pathway can be selectively suppressed during transient shifts of a grating in the surround, consistent with amacrine-mediated suppression of presynaptic OFF bipolar terminals (Geffen et al. 2007).

Asymmetry between ON and OFF pathways

Asymmetries exist between the parallel ON and OFF ganglion cell pathways, for example, in receptive field size and the pattern of excitatory and inhibitory synaptic input (Chichilnisky and Kalmar 2002; Murphy and Rieke 2006; Pang et al. 2003; Sagdullaev et al. 2006; Zaghloul et al. 2003). Here, we found that, in the presence of the grating, OFF cells showed a more consistent suppression of their spike rates and a more consistent membrane hyperpolarization. However, these asymmetries must be interpreted with some caution. For example, we did not systematically explore multiple spatial and temporal frequency conditions for the surround grating, and doing so might reveal conditions that evoke larger suppressive effects in ON cells. Indeed, there were clear cases where ON cells showed suppressive effects, including suppressed spike rates, reduced gain of the subthreshold response and membrane hyperpolarizations (Figs. 4–7). We conclude that different amacrine cell pathways interact with ON and OFF Y cells (i.e., there is not a single ON-OFF amacrine pathway that inhibits both ganglion cell circuits). Consistent with this, in the in vivo rabbit retina, picrotoxin ($GABA_{A/C}$ receptor antagonist) blocked the suppressive effect of a peripheral windmill stimulus for OFF-center Y cells but not ON-center Y cells, which also predicts the involvement of two distinct amacrine cell mechanisms (Caldwell and Daw 1978a).

Peripheral suppression throughout the visual system

Mechanisms for peripheral suppression appear first in the retina but are repeated at several stages of the visual pathway. For example, cells in the lateral geniculate nucleus (LGN) of the thalamus show peripheral suppression (Bonin et al. 2005; Solomon et al. 2002; Webb et al. 2005b). Some of the sup-

pression at the LGN can presumably be explained by a retinal mechanism, but other central mechanisms may also play a role. Peripheral suppression also exists in the primary visual cortex, where its orientation sensitivity, binocular nature and time-course suggest an intracortical mechanism (Bair et al. 2003; DeAngelis et al. 1994; Smith et al. 2006; Webb et al. 2005a). Further surround effects appear in extrastriate areas (see Albright and Stoner 2002; Allman et al. 1985). At all stages, the apparent role of peripheral suppression is to create a context in which to interpret the strength of a central stimulus. It will be interesting to learn whether the circuitry for peripheral suppression described here is repeated at other stages.

ACKNOWLEDGMENTS

We thank D. Green and V. Bonin for comments on the manuscript.

Present address of K. Boahen: Department of Bioengineering, Stanford University, Palo Alto, CA.

GRANTS

This study was supported by National Eye Institute Grants EY-07003, T32-EY-13934, EY-07035, EY-00828, and EY-14454 and the Packard Foundation. J. B. Demb is supported by a Research to Prevent Blindness Career Development Award and an Alfred P. Sloan Research Fellowship.

REFERENCES

Albright TD, Stoner GR. Contextual influences on visual processing. *Annu Rev Neurosci* 25: 339–379, 2002.

Allman J, Miezin F, McGuinness E. Stimulus specific responses from beyond the classical receptive field: neurophysiological mechanisms for local-global comparisons in visual neurons. *Annu Rev Neurosci* 8: 407–430, 1985.

Baccus SA, Meister M. Fast and slow contrast adaptation in retinal circuitry. *Neuron* 36: 909–919, 2002.

Bair W, Cavanaugh JR, Movshon JA. Time course and time-distance relationships for surround suppression in macaque V1 neurons. *J Neurosci* 23: 7690–7701, 2003.

Baldridge WH, Vaney DI, Weiler R. The modulation of intercellular coupling in the retina. *Semin Cell Dev Biol* 9: 311–318, 1998.

Beaudoin DL, Borghuis BG, Demb JB. Cellular basis of contrast gain control over the receptive field center of mammalian retinal ganglion cells. *J Neurosci* 27: 2636–2645, 2007.

Bonin V, Mante V, Carandini M. The suppressive field of neurons in lateral geniculate nucleus. *J Neurosci* 25: 10844–10856, 2005.

Bormann J, Hamill OP, Sakmann B. Mechanism of anion permeation through channels gated by glycine and gamma-aminobutyric acid in mouse cultured spinal neurones. *J Physiol* 385: 243–286, 1987.

Brainard DH. The psychophysics toolbox. *Spat Vis* 10: 433–436, 1997.

Caldwell JH, Daw NW. Effects of picrotoxin and strychnine on rabbit retinal ganglion cells: changes in centre surround receptive fields. *J Physiol* 276: 299–310, 1978a.

Caldwell JH, Daw NW. New properties of rabbit retinal ganglion cells. *J Physiol* 276: 257–276, 1978b.

Carandini M, Demb JB, Mante V, Tolhurst DJ, Dan Y, Olshausen BA, Gallant JL, Rust NC. Do we know what the early visual system does? *J Neurosci* 25: 10577–10597, 2005.

Chander D, Chichilnisky EJ. Adaptation to temporal contrast in primate and salamander retina. *J Neurosci* 21: 9904–9916, 2001.

Chichilnisky EJ. A simple white noise analysis of neuronal light responses. *Network* 12: 199–213, 2001.

Chichilnisky EJ, Kalmar RS. Functional asymmetries in ON and OFF ganglion cells of primate retina. *J Neurosci* 22: 2737–2747, 2002.

Cleland BG, Levick WR. Brisk and sluggish concentrically organized ganglion cells in the cat's retina. *J Physiol* 240: 421–456, 1974.

Cohen ED. Synaptic mechanisms shaping the light-response in retinal ganglion cells. *Prog Brain Res* 131: 215–228, 2001.

Cook PB, Lukasiewicz PD, McReynolds JS. Action potentials are required for the lateral transmission of glycinergic transient inhibition in the amphibian retina. *J Neurosci* 18: 2301–2308, 1998.

Cook PB, McReynolds JS. Lateral inhibition in the inner retina is important for spatial tuning of ganglion cells. *Nat Neurosci* 1: 714–719, 1998.

Cook PB, Werblin FS. Spike initiation and propagation in wide field transient amacrine cells of the salamander retina. *J Neurosci* 14: 3852–3861, 1994.

Dacey DM. Axon-bearing amacrine cells of the macaque monkey retina. *J Comp Neurol* 284: 275–293, 1989.

Dacey D, Packer OS, Diller L, Brainard D, Peterson B, Lee B. Center surround receptive field structure of cone bipolar cells in primate retina. *Vision Res* 40: 1801–1811, 2000.

Dacey DM, Petersen MR. Dendritic field size and morphology of midget and parasol ganglion cells of the human retina. *Proc Natl Acad Sci USA* 89: 9666–9670, 1992.

DeAngelis GC, Freeman RD, Ohzawa I. Length and width tuning of neurons in the cat's primary visual cortex. *J Neurophysiol* 71: 347–374, 1994.

Demb JB, Haarsma L, Freed MA, Sterling P. Functional circuitry of the retinal ganglion cell's nonlinear receptive field. *J Neurosci* 19: 9756–9767, 1999.

Demb JB, Zaghloul K, Haarsma L, Sterling P. Bipolar cells contribute to nonlinear spatial summation in the brisk-transient (Y) ganglion cell in mammalian retina. *J Neurosci* 21: 7447–7454, 2001a.

Demb JB, Zaghloul K, Sterling P. Cellular basis for the response to second-order motion cues in y retinal ganglion cells. *Neuron* 32: 711–721, 2001b.

Dhingra NK, Kao Y-H, Sterling P, Smith RG. Contrast threshold of a brisk-transient ganglion cell in vitro. *J Neurophysiol* 89: 2360–2369, 2003.

Duebel J, Haverkamp S, Schleich W, Feng G, Augustine GJ, Kuner T, Euler T. Two-photon imaging reveals somatodendritic chloride gradient in retinal ON-type bipolar cells expressing the biosensor Clomeleon. *Neuron* 49: 81–94, 2006.

Enroth-Cugell C, Freeman AW. The receptive-field spatial structure of cat retinal Y cells. *J Physiol* 384: 49–79, 1987.

Enroth-Cugell C, Jakiela HG. Suppression of cat retinal ganglion cell responses by moving patterns. *J Physiol* 302: 49–72, 1980.

Enroth-Cugell C, Robson JG. The contrast sensitivity of retinal ganglion cells of the cat. *J Physiol* 187: 517–552, 1966.

Famiglietti EV. Polyaxonal amacrine cells of rabbit retina: morphology and stratification of PA1 cells. *J Comp Neurol* 316: 391–405, 1992.

Flores-Herr N, Protti DA, Wassle H. Synaptic currents generating the inhibitory surround of ganglion cells in the mammalian retina. *J Neurosci* 21: 4852–4863, 2001.

Frishman LJ, Linsenmeier RA. Effects of picrotoxin and strychnine on non-linear responses of Y-type cat retinal ganglion cells. *J Physiol* 324: 347–363, 1982.

Geffen MN, de Vries SEJ, Meister M. Retinal ganglion cells can rapidly change polarity from off to on. *PLoS Biol* 5: e65, 2007.

Hochstein S, Shapley RM. Linear and nonlinear spatial subunits in Y cat retinal ganglion cells. *J Physiol* 262: 265–284, 1976.

Hu EH, Dacheux RF, Bloomfield SA. A flattened retina-eyecup preparation suitable for electrophysiological studies of neurons visualized with transscleral infrared illumination. *J Neurosci Methods* 103: 209–216, 2000.

Kier CK, Buchsbaum G, Sterling P. How retinal microcircuits scale for ganglion cells of different size. *J Neurosci* 15: 7673–7683, 1995.

Kim KJ, Rieke F. Temporal contrast adaptation in the input and output signals of salamander retinal ganglion cells. *J Neurosci* 21: 287–299, 2001.

Kuffler SW. Discharge patterns and functional organization of mammalian retina. *J Neurophysiol* 16: 37–68, 1953.

Lankheet MJ, Prickaerts JH, van de Grind WA. Responses of cat horizontal cells to sinusoidal gratings. *Vision Res* 32: 997–1008, 1992.

Lee YW, Schetzen M. Measurement of the Wiener kernels of a nonlinear system by cross-correlation. *Int J Control* 2: 237–254, 1965.

Lin B, Masland RH. Populations of wide-field amacrine cells in the mouse retina. *J Comp Neurol* 499: 797–809, 2006.

Mangel SC. Analysis of the horizontal cell contribution to the receptive field surround of ganglion cells in the rabbit retina. *J Physiol* 442: 211–234, 1991.

Manookin M, Demb JB. Presynaptic mechanism for slow contrast adaptation in mammalian retinal ganglion cells. *Neuron* 50: 453–464, 2006.

Marmarelis PZ, Marmarelis VZ. *Analysis of Physiological Systems: The White-Noise Approach.* New York: Plenum Press, 1978.

Masland RH. The fundamental plan of the retina. *Nat Neurosci* 4: 877–886, 2001.

McMahon MJ, Packer OS, Dacey DM. The classical receptive field surround of primate parasol ganglion cells is mediated primarily by a non-GABAergic pathway. *J Neurosci* 24: 3736–3745, 2004.

Murphy GJ, Rieke F. Network variability limits stimulus-evoked spike timing precision in retinal ganglion cells. *Neuron* 52: 511–524, 2006.

O'Brien BJ, Isayama T, Richardson R, Berson DM. Intrinsic physiological properties of cat retinal ganglion cells. *J Physiol* 538: 787–802, 2002.

Olveczky BP, Baccus SA, Meister M. Segregation of object and background motion in the retina. *Nature* 423: 401–408, 2003.

Pang JJ, Gao F, Wu SM. Light-evoked excitatory and inhibitory synaptic inputs to ON and OFF alpha ganglion cells in the mouse retina. *J Neurosci* 23: 6063–6073, 2003.

Passaglia CL, Enroth-Cugell C, Troy JB. Effects of remote stimulation on the mean firing rate of cat retinal ganglion cells. *J Neurosci* 21: 5794–5803, 2001.

Peichl L, Gonzalez-Soriano J. Unexpected presence of neurofilaments in axon-bearing horizontal cells of the mammalian retina. *J Neurosci* 13: 4091–4100, 1993.

Peichl L, Ott H, Boycott BB. Alpha ganglion cells in mammalian retinae. *Proc R Soc Lond B Biol Sci* 231: 169–197, 1987.

Pelli DG. The VideoToolbox software for visual psychophysics, transforming numbers into movies. *Spat Vis* 10: 437–442, 1997.

Rieke F. Temporal contrast adaptation in salamander bipolar cells. *J Neurosci* 21: 9445–9454, 2001.

Robertson B. Characteristics of GABA-activated chloride channels in mammalian dorsal root ganglion neurones. *J Physiol* 411: 285–300, 1989.

Rodieck RW. Quantitative analysis of cat retinal ganglion cell response to visual stimuli. *Vision Res* 5: 583–601, 1965.

Roska B, Werblin F. Vertical interactions across ten parallel, stacked representations in the mammalian retina. *Nature* 410: 583–587, 2001.

Roska B, Werblin F. Rapid global shifts in natural scenes block spiking in specific ganglion cell types. *Nat Neurosci* 6: 600–608, 2003.

Sagdullaev BT, McCall MA, Lukasiewicz PD. Presynaptic inhibition modulates spillover, creating distinct dynamic response ranges of sensory output. *Neuron* 50: 923–935, 2006.

Sakai HM, Naka K. Signal transmission in the catfish retina. IV. Transmission to ganglion cells. *J Neurophysiol* 58: 1307–1328, 1987.

Sakai HM, Wang JL, Naka K. Contrast gain control in the lower vertebrate retinas. *J Gen Physiol* 105: 815–835, 1995.

Schwartz EA. Organization of on-off cells in the retina of the turtle. *J Physiol* 230: 1–14, 1973.

Shapley RM, Victor JD. Nonlinear spatial summation and the contrast gain control of cat retinal ganglion cells. *J Physiol* 290: 141–161, 1979.

Shields CR, Lukasiewicz PD. Spike-dependent GABA inputs to bipolar cell axon terminals contribute to lateral inhibition of retinal ganglion cells. *J Neurophysiol* 89: 2449–2458, 2003.

Smith MA, Bair W, Movshon JA. Dynamics of suppression in macaque primary visual cortex. *J Neurosci* 26: 4826–4834, 2006.

Solomon SG, Lee BB, Sun H. Suppressive surrounds and contrast gain in magnocellular-pathway retinal ganglion cells of macaque. *J Neurosci* 26: 8715–8726, 2006.

Solomon SG, White AJ, Martin PR. Extraclassical receptive field properties of parvocellular, magnocellular, and koniocellular cells in the primate lateral geniculate nucleus. *J Neurosci* 22: 338–349, 2002.

Stafford DK, Dacey D. Physiology of the A1 amacrine: a spiking, axon-bearing interneuron of the macaque monkey retina. *Vis Neurosci* 14: 507–522, 1997.

Sterling P, Demb JB. Retina. In: *Synaptic Organization of the Brain* (5th ed.), edited by Shephard G. New York: Oxford, 2004, p. 217–269.

Taylor WR. TTX attenuates surround inhibition in rabbit retinal ganglion cells. *Vis Neurosci* 16: 285–290, 1999.

Thibos LN, Werblin FS. The properties of surround antagonism elicited by spinning windmill patterns in the mudpuppy retina. *J Physiol* 278: 101–116, 1978.

Vaney DI, Peichl L, Boycott BB. Neurofibrillar long-range amacrine cells in mammalian retinae. *Proc R Soc Lond B Biol Sci* 235: 203–219, 1988.

Victor JD. The dynamics of the cat retinal X cell centre. *J Physiol* 386: 219–246, 1987.

Volgyi B, Xin D, Amarillo Y, Bloomfield SA. Morphology and physiology of the polyaxonal amacrine cells in the rabbit retina. *J Comp Neurol* 440: 109–125, 2001.

Wässle H. Parallel processing in the mammalian retina. *Nat Rev Neurosci* 5: 747–757, 2004.

Webb BS, Dhruv NT, Solomon SG, Tailby C, Lennie P. Early and late mechanisms of surround suppression in striate cortex of macaque. *J Neurosci* 25: 11666–11675, 2005a.

Webb BS, Tinsley CJ, Vincent CJ, Derrington AM. Spatial distribution of suppressive signals outside the classical receptive field in lateral geniculate nucleus. *J Neurophysiol* 94: 1789–1797, 2005b.

Werblin FS. Lateral interactions at inner plexiform layer of vertebrate retina: antagonistic responses to change. *Science* 175: 1008–1010, 1972.

Werblin FS, Copenhagen DR. Control of retinal sensitivity. 3. Lateral interactions at the inner plexiform layer. *J Gen Physiol* 63: 88–110, 1974.

Wiener N.*Nonlinear Problems in Random Theory.* New York: Wiley, 1958.

Yin L, Smith RG, Sterling P, Brainard DH. Chromatic properties of horizontal and ganglion cell responses follow a dual gradient in cone opsin expression. *J Neurosci* 26: 12351–12361, 2006.

Zaghloul KA, Boahen K, Demb JB. Different circuits for ON and OFF retinal ganglion cells cause different contrast sensitivities. *J Neurosci* 23: 2645–2654, 2003.

Zaghloul KA, Boahen K, Demb JB. Contrast adaptation in subthreshold and spiking responses of mammalian Y-type retinal ganglion cells. *J Neurosci* 25: 860–868, 2005.